**2020 SCEC Annual Report #20072**
**Deriving shallow structure from co-located broadband seismic and pressure data**
**Period: 2/1/2020-1/31/2021**

**PI : Toshiro Tanimoto (UC Santa Barbara)**

## 1.Project Objective

We developed an inversion method for deriving shallow elastic structure from co-located pressure and seismic data. Such co-located stations have rapidly increased in the last 10 years, including the EarthScope Transportable Array. We have tested the method by comparing our results for Vs30 against independent Vs30 measurements by other studies. During 2020, we improved this inversion method and applied it to the EarthScope data and selected stations in Southern California.

## 2.Method and Background Phenomenon

### (2.1) Background phenomena

In the frequency range 0.01-0.05 Hz, the coupling between the atmosphere (pressure) and solid Earth can become large when surface pressure variations become large. Figure 1 (Left) shows raw coherence values between pressure and vertical seismic velocity data from the first 30 days in 2014. Figure 1 (right) shows an annual average. They indicate that when pressure is high, coherence can be quite high for frequencies between about 0.01 Hz and 0.05 Hz. Based on this, we focus our analysis on this frequency range, particularly choosing the high-pressure time intervals.

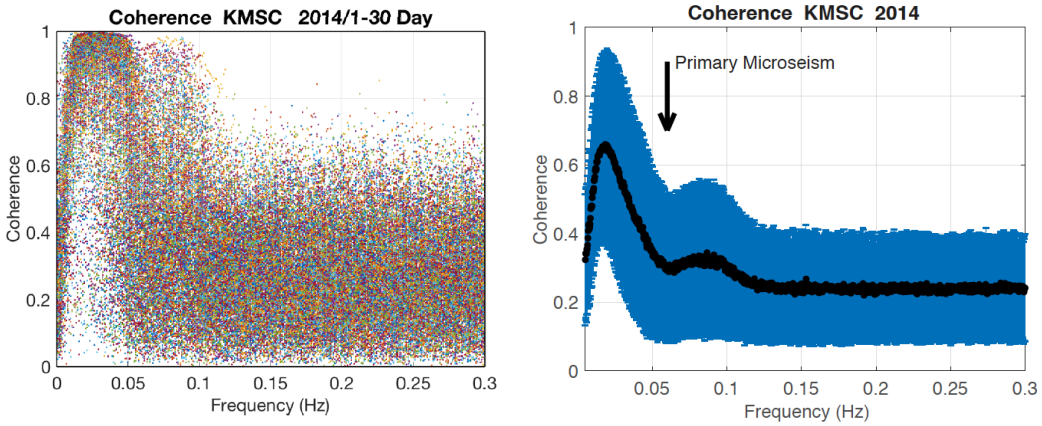


**Figure 1: (Left) Raw coherence at station KMSC in South Carolina from the first 30 days in 2014. The coherence between pressure and vertical seismic velocity data was computed for each 1-hour time interval. Different colors mean different 1-hour time series. (Right) Annual average of coherence. Effects of the ocean-generated microseism weakens coherence at about 0.06 Hz, but atmospheric effects exist up to about 0.12 Hz.**

Figure 2 (left) shows the seismic PSDs plotted against pressure PSDs at 0.02 Hz for an ErathScope station U57A. Vertical seismic PSDs are in blue and horizontal PSDs (sum of two directions) are in red. Vertical PSDs show a near-constant (flat) range for pressure PSDs below 1 $Pa^2$/Hz where seismic PSDs do not vary with Pressure PSDs. But above this pressure (1 $Pa^2$/Hz), the vertical PSD becomes proportional to the pressure PSD, indicating that local pressure becomes the controlling source for seismic noise above about pressure 1 $Pa^2$/Hz. In the right panel (Figure 2), the time intervals with coherence higher than 0.7 are indicated by green points. High-coherence (green) points are found mainly above 1 $Pa^2$/Hz and confirms the fact that when surface pressure is the controlling source, pressure and seismic data become highly coherent.

Figure 3 shows phase shifts between pressure and vertical displacement at three stations (bottom panels). It shows that pressure and vertical displacement have opposite signs; when pressure is high, surface is depressed downward and vice versa. The surface is going up and down with surface pressure with opposite signs, as illustrated in Figure 3. In this situation, the solid Earth is responding to surface pressure changes and the ratio $\eta(f) = S_z/S_p$ should give us a measure of its elastic response. From colocated data, we measure this quantity between 0.01 Hz and 0.05 Hz and invert for elasticity of shallow structure.

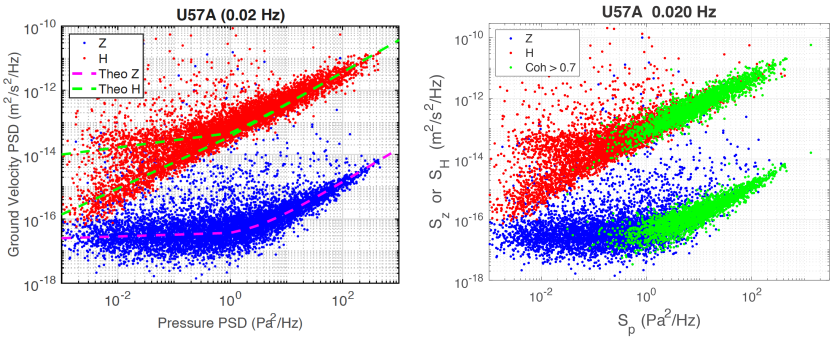


**Figure 2: (Left) Seismic velocity PSDs plotted against pressure PSDs at 0.02 Hz. Vertical PSDs in blue and horizontal PSDs (sum of two components) in red. Vertical PSDs have a threshold pressure PSD at about 1 Pa²/Hz above which the vertical PSDs and pressure PSDs become correlated. (Right) Same station with the left panel except that time intervals with coherence higher than 0.7 are indicated by green.**

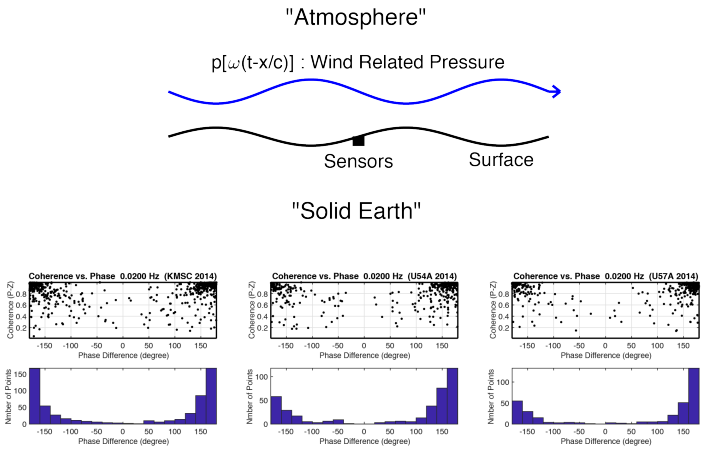


**Figure 3: When pressure and vertical data are coherent, phase shifts between vertical displacement and pressure are 180 degrees (shown at three different stations), suggesting the situation in the upper panel. The top panel indicates that when pressure is high, the surface is depressed downward and vice versa. Earth's surface is literally responding to the local pressure.**

### (2.2) Example of Results for nine stations at Pinyon Flat Observatory (PFO)

We developed an inversion procedure (Tanimoto and Wang, 2019). We show an example of inversion for station BPH07 (at PFO). The whole inversion process is based on the relationship given by

$$\frac{\delta\eta}{\eta} = \int \{K_\kappa \frac{\delta\kappa}{\kappa} + K_\mu \frac{\delta\mu}{\mu}\}\, dz$$

where the misfit between data and theory ($\delta\eta$) is solved for perturbations in bulk modulus ($\delta\kappa$) and shear modulus ($\delta\mu$). Density effects are quite small because of the quasi-static nature of this phenomenon (Tanimoto and Wang, 2019).

Figure 4 shows an example of inversion for station BPH07. The left panel shows $\eta(f)$ measured from data. The starting model was created by a procedure in Tanimoto and Wang (2019) and led to blue lines for the structure (Figure 4, middle) and the fit (Figure 4, left). The middle panel shows the starting model was already quite good. The starting model (blue) and the inverted models (rigidity and bulk modulus) for the first iteration (green) and the second iteration (red) are shown in Figure 4 (middle two panels). The inversion converged at the second iteration. The final model shows that data require a low ridigity layer in the upper 20 m of the crust. The SCEC CVMH model has the surface rigidity about 1 GPa. This result thus shows that there is a lower rigidity layer by 20-30 percent in the top 20 m. Density (unchanged from the starting model), Vp and Vs structure are shown in the right panel.

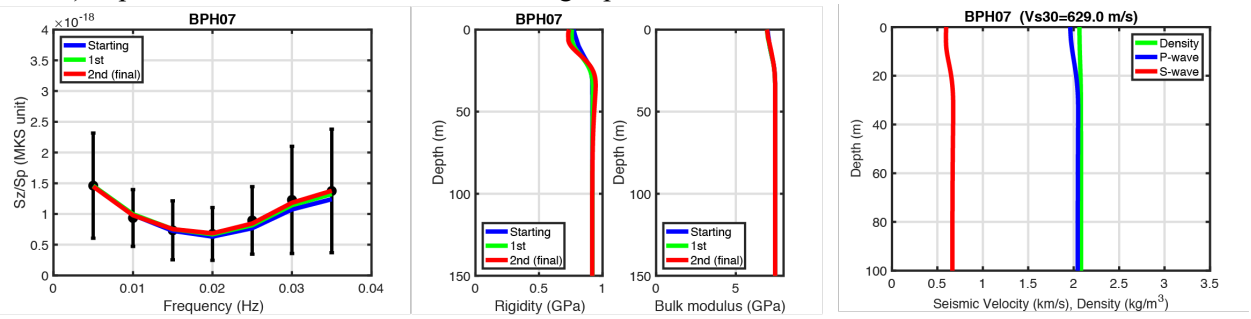


**Figure 4: (Left) Measured$\eta(f)$ and their uncertainties (1σ). Fit by the starting model (blue), the 1st iteration model (green) and the 2nd iteration model (red).The second-iteration model is the final model. (Middle) Rigidity and bulk modulus models are shown. (Right) Density, P-wave speed and S-wave speed for the final model. Computed Vs30 for this model is 629 m/s.**

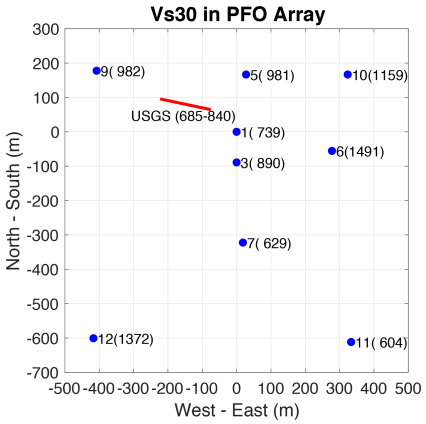


**Figure 5: Vs30 derived for 9 stations at PFO using analysis for the low frequency range (0.01-0.05 Hz). Each co-located station is shown by blue circle and the number in parenthesis is our estimate for Vs30. Yong et al. (2016) estimated 685-841 m/s using the geophone array, located along the red line.**

We applied our low-frequency approach to nine co-located data at the Piñon Flat Observatory. The primary purpose is to compare our Vs30 against other estimates. Figure 5 shows the Vs30 values that we derived from our inversion results. Blue cirlces indicate the location of co-located stations. For example, 9 (982) near the upper left corner means that Vs30 at station BPH09 is 982 m/s. The red line indicates the location of a study by Yong et al. (2016) which used dense geophone arrays. Their estimates (685-840 m/s) roughtly agree with our results for the nearest station BPH01 (739 m/s) but differ from BPH05 (981 m/s) and BPH09 (982 m/s). These spatial variation indicates that thickness of shallow sedimentary layer changes at short lateral distances, on the order of about 100 m.

## 3. Results

### (3.1) EarthScope Transportable Array

From the beginning, the EarthScope Transportable Array had high-quality broadband sensors but lacked high-quality pressure sensors. But since about 2012, high-quality barometers (Setra) and infrasound sensors (Hyperion) were added to measure pressure. Both pressure sensors can provide highly accurate pressure measurements for the frequency range 0.01-0.05 Hz.

One of our achievem,ents in 2020 was estimates of Vs30 for all available co-located TA stations from 2012 to 2019. We applied a simple half-space invresion method (Wang and Tanimoto, 2020) as well as a layered structure inversion for each station site. Figure 6 shows our Vs30 estimates. Strictly speaking, our approach derives depth variation of elastic moduli beneath a station. We then use empirical relations (Boore, 2016) to convert to seismic velocity structures.

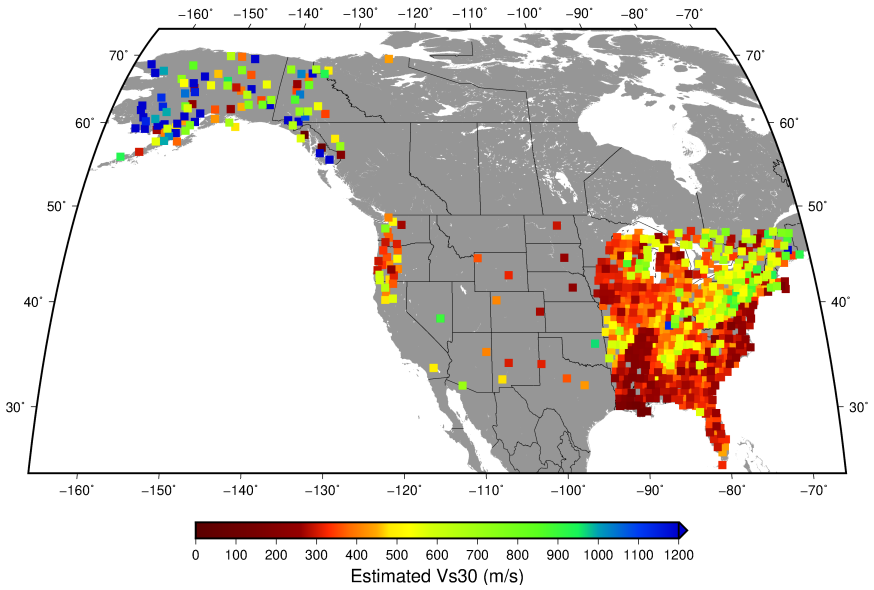


**Figure 6: Vs30 estimated by layered inversion for EarthScope stations 2012-2018. Scale is saturated at 1200 m/s. Wang and Tanimoto (2021).**

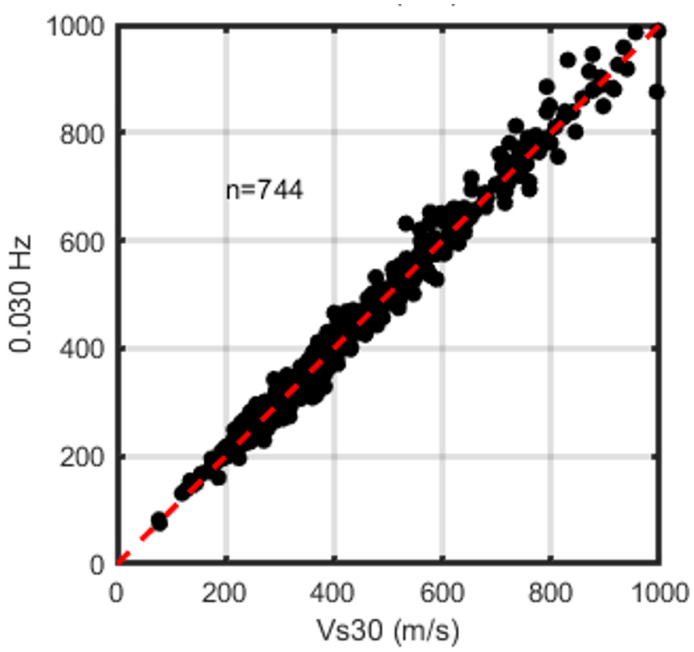

**Figure 7: Comparison of Vs30 derived by a homogeneous half-space method (the ordinate) and by a layered inversion method.**

Comparison with our previous results by a simple homogeneous half-space model is shown in Figure 7, which shows reasonable agreements between the two methods. But the results by layered inversions provide more insights into the depth variations of elasticity. Depth resolution analysis is not possible for half-space approach. The results for the layered inversion is being written up for publication.

### (3.2) Selected Southern California Stations

We found that some stations in Southern California had pressure sensors between about 2000 and 2010. Since our approach requires that pressure and seismic sensors must be close, typically within a few to 10m, some stations did not qualify as co-located stations. But we judged that six stations in the Table 1 can be viewed as co-located stations.

Figure 8 shows an example of inversion for USC. Data look quite good and the goodness of fit to Sz/Sp (the top-left panel) appear quite good. Our Vs30 result is 145 (m/s) for this site and is much smaller than 350 (m/s) obtained by Yong et al. (2016). In fact, for all six stations, our approach resulted in systematicaly small Vs30 in comparison to Vs30 estimates by Yong et al. (2016). Our results agreed with Yong et al.'s at PFO (Figure 5). This might have been caused by modern higher quality pressure sensors at PFO but we have not quite understood these systematic differences in Table 1.

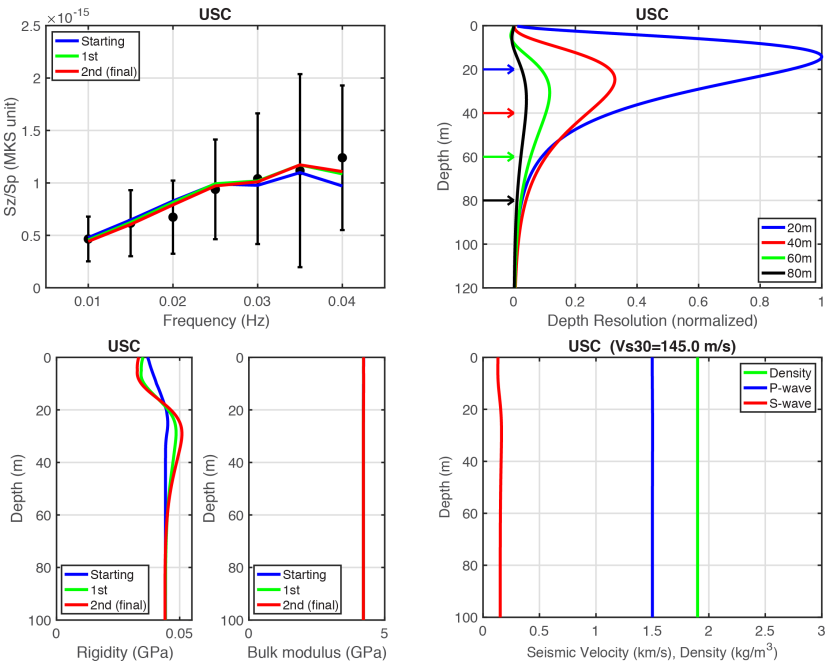


**Figure 8: Analysis at USC. (top-left) Goodness of fit. (top-right) Depth resolutions at target depths. (bottom-left) Shear-modulus and bulk-modulus in the upper 100m. (bottom-right) Converted seismic structure.**

**Table 1: Vs30 for Stations in Southern California. Pressure sensors during the years 2000-2010. Station names (left), Vs30 by Yong et al. (2016) and our Vs30 estimates (right).**

| Station | Vs30 (Yong et al.) (m/s) | Vs30 (Our approach) (m/s) |
|---|---|---|
| BAR | 559 | 215 |
| MLAC | 322 | 218 |
| SNCC | 668 | 242 |

| | | |
|---|---|---|
| PAS | 638 | 349 |
| RPV | 573 | 199 |
| USC | 350 | 145 |

**References**

Tanimoto, T. and J. Wang (2018), Low-frequency seismic noise characteristics from the analysis of co-located seismic and pressure data, Journal of Geophysical Research: Solid Earth, 123, 2018. doi:10.1029/2018JB015519

Tanimoto, T. and J. Wang (2019), Theory for deriving shallow elasticity structure from collocated seismic and pressure data, Journal of Geophysical Research: Solid Earth, 124, 5811-5835, doi:10.1029/2018JB017132

Tanimoto, T. and J. Wang (2020), Shallow elasticity structure from colocated pressure and seismic stations in the Pinyon Flat Observatory and estimation of Vs30, Geophys. J. Int., 222, 678-696, doi:10.1093/gji/ggaa195

Wang, J. and T. Tanimoto (2020), Estimating near-surface rigidity from low-frequency noise using collocated pressure and horizontal seismic data, Bull. Seism. Soc. Am., XX, 1-11. doi:10.1785/0120200098

Yong, A., E. Thompson, D. Wald, K. Knudsen, J. Odum, W. Stephenson, and S. Haefner (2016), Compilation of Vs30 data for the United States: U. S. Geological Survey Data Series 978, 8p., http://dx.doi.org/10.3133/ds978.